Journal of Experimental and Clinical Application of Chinese Medicine

ORIGINAL RESEARCH

Open Access

Chemical Constituents of the Alpine Bistort Rhizome and Network Pharmacology Study on Its Anti-diarrheal Effects

Chao Zhang [1,2,#], Mengqi Wu [1,2,#], Qi Huang [1], Jiasheng Xie [3], Zhuobin He [1], Weiqi Yang [1], Jiaqi Fang [1], Xiaoqian Shen [1], Zhengming Qian [1,2,*]

1. Dongguan HEC Cordyceps R&D Co., Ltd., 523871 Dongguan, Guangdong, China
2. Yichang Shanchengshuidu Cordyceps Co., Ltd., 443000 Yichang, Hubei, China
3. Guangdong Mige Sunshine Technology Co. Ltd., 510700 Guangzhou, Guangdong, China

# The authors contributed equally to this work.

DOI: https://doi.org/10.62767/jecacm701.1819

Keywords

Alpine bistort rhizome

Chemical composition

Diarrhea

Network pharmacology

Molecular docking

* **Correspondence**

Zhengming Qian

Dongguan HEC Cordyceps R&D Co., Ltd., 523871 Dongguan, Guangdong, China; Yichang Shanchengshuidu Cordyceps Co., Ltd., 443000 Yichang, Hubei, China

E-mail: qianzhengming1982@126.com

Received: 22 December 2025

Revised: 9 February 2026

Accepted: 13 March 2026

Published: 27 March 2026

Journal of Experimental and Clinical Application of Chinese Medicine **2026; 7(1): 27-54.**

Abstract

To systematically analyze the antidiarrheal active components and potential mechanisms in the rhizome of alpine bistort (*Bistorta vivipara* (L.) Gray). This study separated and identified 9 categories of chemical components in the alpine bistort rhizome employing methods such as high-performance liquid chromatography (HPLC), high-performance liquid chromatography-evaporative light scattering detection (HPLC-ELSD), high-performance liquid chromatography-mass spectrometry (HPLC-MS), gas chromatography-mass spectrometry (GC-MS), inductively coupled plasma mass spectrometry (ICP-MS), etc. A total of 126 chemical components were identified from the samples of alpine bistort rhizome, including 4 polysaccharides, 6 monosaccharides that compose polysaccharides, 3 free sugars, 17 amino acids, 3 nucleosides, 2 sterols, 14 organic acids, 21 flavonoids, 2 glycosides, 1 Sugar-conjugated polymer, 34 volatile components, and 19 elements.The main chemical components, targets, and potential signaling pathways of alpine bistort rhizome for preventing diarrhea were screened using network pharmacology methods, and molecular docking was performed on key compounds and targets. The results showed that 50 active components in alpine bistort rhizome could regulate the Tumor Necrosis Factor (TNF) signaling pathway, lipid and atherosclerosis , Phosphoinositide 3-Kinase-Protein Kinase B (PI3K-Akt) signaling pathway and Hypoxia-Inducible Factor-1 (HIF-1) signaling pathway by acting on 227 target points, thus exerting the anti-diarrhea effect. The molecular docking results revealed that the core targets Signal Transducer and Activator of Transcription 3 (STAT3), Epidermal Growth Factor Receptor (EGFR), TNF, Heat shock protein 90kDa alpha (cytosolic), class A member 1 (HSP90AA1), and Recombinant Caspase 3 (CASP3) exhibited good binding ability with the active compounds.This study preliminarily elucidated the pharmacological basis of the rhizome of alpine bistort and its potential mechanism, providing a scientific foundation for its clinical application and quality control.

1 Introduction

Alpine bistort, *Bistorta vivipara* (L.) Gray, a perennial herb of genus *Bistorta* in the Polygonaceae family, is mainly rooted in Qinghai, Xizang, Sichuan, and Gansu in China, and mostly grows in the undergrowth of hillsides, alpine, or subalpine meadows at an altitude of 1200-5100 m [1-3]. Alpine bistort, as an important feed for the host insects of the precious Chinese medicinal herb *Ophiocordyceps sinensis*, has a special ecological status in the high-altitude ecosystem [4,5]. Its dried rhizome is the traditional medicinal herb "Ranbu" in Xizang, with a medicinal history spanning thousands of years, which has antidiarrheal, stomachic, and emmenagogue properties, and is commonly used to treat various diseases such as stomach diseases, indigestion, diarrhea, and menstrual disorders [6,7]. Modern research has proved that the alpine bistort rhizome contains various components such as flavonoids, phenols, and polysaccharides [8], possessing anti-diarrheal, anti-inflammatory, anticancer, and antioxidant effects [9-11]. Diarrhea is a common digestive system disease, mainly resulting from infectious pathogens, food allergies, or intestinal diseases [12]. Due to its potent anti-diarrheal properties, alpine bistort rhizome has been used to develop formulations such as Zhuyaliao Zhixie Granules and Zhuyaliao Zhixie Capsules. Clinical studies have confirmed their significant efficacy in alleviating pediatric diarrhea symptoms and reducing bowel movements [13-16]. However, since alpine bistort rhizome has complex components, the key active components, targets, and specific mechanisms of its anti-diarrheal effects have not yet been elucidated.

Network pharmacology, an emerging interdisciplinary field based on systems biology theory, reveals the molecular-level mechanism of drugs by constructing a complex drug-component-target-disease network relationship [17]. Network pharmacology systematically analyzes the synergistic effects of multiple components and targets in drugs primarily using network topological computing, clustering analysis, and visualization techniques [18,19]. This method is particularly applicable to the research of complex systems of traditional Chinese medicine (TCM) [20,21], which not only can clarify the material basis of TCM and compound preparations in treating diseases, but also can predict the regulatory mechanism of signaling pathways and be used for clinical application and development of new drugs, quality control of TCM and toxicology research [22]. This study will reveal the active components, therapeutic core targets, and main signaling pathways of alpine bistort rhizome in preventing diarrhea using network pharmacology methods, and virtually verify and screen active components and core targets through molecular docking technology, in order to provide scientific references for deeply exploring the mechanism of alpine bistort rhizome in preventing diarrhea, and theoretical basis for the clinical application and new drug development of alpine bistort rhizome.

2 Materials and methods

2.1 Materials

The sample information of the alpine bistort rhizome is shown in Table 1. The samples were identified by Dr. Zhengming Qian, a TCM pharmacist, as the plant of genus Bistorta in the Polygonaceae family.

Table 1 Sample information of the alpine bistort rhizome.

Number of samples	Place of origin	Time of sampling
S01	Bijie, Guizhou	2024.06.06
S02	Xichang, Sichuan	2024.06.28
S03	Zhaotong, Yunnan	2024.06.13

2.2 Reagents

The controls, including glucose (Lot: 110833-202410), mannose (Lot: 140651-202206), uridine (Lot: 110887-202305), and guanosine (Lot: 111977-202202), were purchased from the National Institutes for Food and Drug Control. Dextran controls (1000 Da, 12000 Da, 80000 Da, 150000 Da, 410000 Da, 670000 Da; Lot: BCBW9414, BCBW9405, BCBT2281, BCBW9409, BCBZ3885, BCBW3821, respectively) were obtained from Sigma-Aldrich (Shanghai) Trading Co., Ltd. Controls of rhamnose (Lot: 32800), galactose (Lot: F2215342), fucose (Lot: F1924062), arabinose (Lot: C1517114), fructose (Lot: K1830110), sucrose (Lot: K1814122), adenine (Lot: E1814056), cholesterol (Lot: C2404218), and stigmasterol (Lot: E1405007) were ordered from Shanghai Aladdin Biochemical Technology Co., Ltd. The cytidine control (Lot: 220902) was acquired from Shanghai Winherb Medical Science Co., Ltd. Controls of asparagine (Lot: BCBH3779V), glutamine (Lot: BCBV9035), and tryptophan (Lot: BCBV3938) were sourced from Agilent Technologies, Inc. The amino acid standard H (Lot: UL290479), ergosterol (Lot: 2421679), and sitosterol (Lot: 3389) were obtainable from Thermo Fisher Scientific Inc., ANPEL Laboratory Technologies (Shanghai) Inc., and Shanghai Nature Standard Biotech Co., Ltd., respectively. Single-element standard solutions of Cr (Lot: 249018), As (Lot: 24D40035), Cd (Lot: 2405024), Hg (Lot: 24D51281), Pb (Lot: 24D51500), Cu (Lot: 245016), Au (Lot: 231111), Se (Lot: 22B040-2), Mo (Lot: 228030-2), Sn (Lot: 22A038-4), K (Lot: 22A039-3), Ca (Lot: 224012-2), Na (Lot: 224037-8), Mg (Lot: 244015-4), Al (Lot: 228021-6), Fe (Lot: 227027-7), P (Lot: 231005-4), Ni (Lot: 231029-2), Sc (Lot: 23C041), Ge (Lot: 23C039-2), In (Lot: 23C016), and Bi (Lot: 23B019-2), as well as a 23 multi-element mixed metal standard solution (Lot: 23D50707), were acquired from the National Analysis Center for Nonferrous Metals and Electronic Materials. Anhydrous ethanol (Lot: KEKF8003) and anhydrous methanol (Lot: ABKET069) were purchased from Beijing InnoChem Science & Technology Co., Ltd. Ammonium acetate (Lot: 2022030401), sodium hydroxide (Lot: B2312180), dichloromethane (Lot: 180921), sodium dihydrogen phosphate dihydrate (Lot: B2305051), disodium hydrogen phosphate dodecahydrate (Lot: B2308111), and potassium hydroxide (Lot: B2303181) were procured from Xilong Scientific Co., Ltd. Trifluoroacetic acid (Lot: C2006129), 1-phenyl-3-methyl-5-pyrazolone (PMP, Lot: K1820098), 9-fluorenylmethyl chloroformate (FMOC, Lot: H142111), o-phthalaldehyde (OPA, Lot: B1504093), 3-mercaptopropionic acid (Lot: C1602147), sodium tetraborate decahydrate (Lot: D1804033), and phosphoric acid (Lot: B2211254) were purchased from Shanghai Aladdin Biochemical Technology Co., Ltd. Hydrochloric acid (Lot: 2021062801) was purchased from Chengdu Kelong Chemical Co., Ltd. Concentrated nitric acid (Lot: G220305) was ordered from Dongguan Kangrun Experimental Technology Co., Ltd. All the above reagents were of analytical grade. Chromatographic grade acetonitrile (Lot: D531737) and methanol (Lot: D911526) were obtained from ANPEL Laboratory Technologies (Shanghai) Inc. Chromatographic grade formic acid (Lot: I2110246) was purchased from Shanghai Aladdin Biochemical Technology Co., Ltd.

2.3 Instruments

High-performance liquid chromatograph (HPLC) (1260, Agilent Technologies, Inc., California, USA); Evaporative Light-Scattering Detector (ELSD) (1260 Ⅱ, Agilent Technologies, Inc., California, USA); Quadrupole-Time of Flight (Q-TOF) mass spectrometer (6545, Agilent Technologies, Inc., California, USA); gas chromatography-mass spectrometry (GC-MS) (7890B-5977B, Agilent Technologies, Inc., California, USA); inductively coupled plasma mass spectrometry (ICP-MS) (8800,

Agilent Technologies, Inc., California, USA); ultrasonic cleaner (P300H, Elma Schmidbauer GmbH, Baden-Württemberg , Germany).

2.4 Methods

2.4.1 Analysis of molecular weight of polysaccharide

Control solution preparation: approximately 10 mg each of glucose and dextrans (1000 Da, 5000 Da, 12000 Da, 25000 Da, 50000 Da, 80000 Da, 150000 Da, 270000 Da) were accurately weighed, placed in a 20 mL volumetric flask, dissolved and diluted to indicated scale with water, followed by mixing to obtain the solution.

Test solution preparation: approximately 0.5 g of the sample powder was added into 20 mL of water, followed by reflux in a boiling water bath for 4 h. The sample was transferred to a 50 mL centrifuge tube and centrifuged for 20 min (5000 rpm). 5 mL of the supernatant was precisely pipette. 20 mL of anhydrous ethanol was added and mixed thoroughly. The mixture was placed in a 4 ℃ refrigerator overnight. The next day, the mixture was centrifuged for 15 min (5000 rpm), the supernatant was discarded, and the precipitate was dried until no alcohol odor remained. The precipitate was precisely dissolved in 10 mL of water, and filtered through a 0.22 μm membrane to obtain the test sample solution.

Chromatographic conditions: TSKgel Super Multipore PW-H chromatographic column (150 mm × 6.0 mm, 8 μm); mobile phase: 0.1 mol/L ammonium acetate underwent isocratic elution with a flow rate of 0.4 mL/min; column temperature: 35 ℃ ; injection volume: 20 μL; the carrier gas of ELSD detector: nitrogen; carrier gas pressure: 3.5 bar; temperature of drift tube: 60 ℃; Gain: 6; Filter: 6.

Linear regression analysis was conducted using the logarithm of the molecular weight of dextran and the retention time to establish the molecular weight calibration curve. Based on the retention times of the chromatographic peaks in the test sample solution, the corresponding molecular weights were determined using the calibration curve.

2.4.2 Analysis of monosaccharide composition of polysaccharides

Control solution preparation: appropriate amounts of mannose, glucose, galactose, and arabinose controls were dissolved in water, and prepared into a mixed control solutions with concentrations of 21 μg/mL, 52 μg/mL, 20 μg/mL, and 53 μg/mL. Appropriate amounts of rhamnose and fucose controls were dissolved in water, and prepared into a mixed control solutions with concentrations of approximately 10 μg/mL.

Test solution preparation: 0.5 g sample powder was added with 20 mL of water, followed by reflux in a boiling water bath for 4 h. The sample was transferred to a 50 mL centrifuge tube, and centrifuged for 5 min (5000 rpm). 5 mL of the supernatant was mixed with 20 mL of anhydrous ethanol and placed in a 4 ℃ refrigerator overnight. The next day, after centrifugation for 15 min (5000 rpm), the supernatant was discarded, and the precipitate was dried until no alcohol odor remained. 10 mL of water was added for dissolution. 1 mL of the above solution and 1 mL of 4 mol/L trifluoroacetic acid solution were co-hydrolyzed in a 100 ℃ oven for 2 h. After being cooled to room temperature, the sample was evaporated to dryness under nitrogen stream, then added with 1 mL of methanol and evaporated to dryness under nitrogen stream again. This process was repeated three times. The residue was dissolved in 1 mL of water to obtain the test solution.

Derivatization: 100 μL of the mixed control solution and the test solution were transferred into 2 mL centrifuge tubes, and mixed well with 50 μL of 0.6 mol/L NaOH solution and 100 μL of 0.6 mol/L PMP methanol solution, followed by being sealed and reacted in a 70 ℃ water bath for 60 min. The samples

were cooled to room temperature. 100 μL of 0.3 mol/L HCl solution was added for neutralization, and then 650 μL of ultrapure water was added for thorough mixing. 500 μL of the resulting solution was transferred into a 2 mL centrifuge tube, and underwent 1-min vortex with 1 mL of dichloromethane. Following 5-min centrifugation (12,000 rpm), the supernatant was collected and filtered through a 0.22 μm membrane for analysis.

Chromatographic conditions: Agilent Zorbax SB-C18 column (150 mm × 4.6 mm, 5 μm); mobile phase A: 0.01 mol/L ammonium acetate (pH = 5.5), mobile phase B: acetonitrile; gradient elution: 0-22 min, 15%-25% B; 22 – 25 min, 25% B; 25-27 min, 25%-50% B; 27-37 min, 50% B; 37-40 min, 50%-15% B; flow rate: 1 mL/min; column temperature: 25 ℃; injection volume: 5 μL; detection wavelength: 254 nm.

2.4.3 Analysis of free sugars

Control solution preparation: appropriate amounts of glucose, fructose, and sucrose were dissolved in water to prepare control solutions with concentrations of 104.9 μg/mL, 106.5 μg/mL, and 1293.0 μg/mL, respectively.

Test solution preparation: approximately 0.1 g of the sample powder was added with 20 mL of 70% ethanol, and underwent reflux in a boiling water bath for 1 h. The supernatant was filtered through a 0.22 μm membrane, and the filtrate was used as the test solution.

Chromatographic conditions: Shodex Asahipak NH2P-50 4E column (250 mm × 4.6 mm, 5 μm); water as mobile phase A and acetonitrile as mobile phase B, with gradient elution: 0-20 min, 80% B; 20-30 min, 80%-60% B; flow rate: 1 mL/min; column temperature: 30 ℃; injection volume: 15 μL; ELSD detector parameters: carrier gas nitrogen; gas flow rate: 1.8 SLM; evaporation temperature: 45 ℃; nebulization temperature: 45 ℃; gain value: 1.

2.4.4 Amino acid analysis

Solution preparation: FMOC solution: approximately 20 mg of FMOC was dissolved in 8 mL of acetonitrile, and mixed well. OPA solution: approximately 81 mg of OPA was dissolved in 7 mL of 0.4 mol/L phosphate buffer solution, and then mixed well with 1 mL of acetonitrile and 125 μL of 3-mercaptopropionic acid. Diluent: 100 mL of an aqueous solution containing 10 mM Na_2HPO_4 and 10 mM $Na_2B_4O_7$ (pH = 8.2) were mixed with 0.4 mL of phosphoric acid.

Control solution preparation: appropriate amounts of norvaline and sarcosine were dissolved in water, and prepared into an internal standard solution with a concentration of 5 mmol/L. Appropriate amounts of asparagine, glutamine, tryptophan, and the amino acid standard H were dissolved in water, and prepared into a mixed control solution with a concentration of 0.25 mmol/L. 0.9 mL of the above mixed solution and 0.1 mL of the internal standard solution were mixed well to obtain the final control solution.

Free amino acid test solution preparation: 0.2 g of sample powder was mixed with 5 mL of water, and performed ultrasonic extraction for 30 min. The supernatant was filtered through a 0.22 μm membrane. 0.9 mL of the subsequent filtrate was added with 0.1 mL of the internal standard solution, and mixed well to obtain the test solution.

Hydrolyzed amino acid test solution preparation: 0.2 g sample powder was sealed with 6 mL of 6 mol/L hydrochloric acid solution, and hydrolyzed in an oven at 110 ℃ for 24 h. The solution was transferred to an evaporation dish, and the gas-phase vial was rinsed multiple times with 25 mL of water. The washing liquid was added into the evaporation dish and dried. The residue was washed multiple times with 0.02 mol/L hydrochloric acid solution, and placed into a 50 mL volumetric flask with washing liquid. 0.02 mol/L

hydrochloric acid solution was added for obtain constant volume, mixed well and filtered through a 0.22 μm membrane. 0.9 mL of the subsequent filtrate was mixed with 0.1 mL of internal standard solution to obtain the test solution.

Chromatographic conditions: AdvanceBio AAA C18 column (100 mm × 4.6 mm, 2.7 μm); mobile phase A: aqueous solution containing 10 mM Na_2HPO_4 and 10 mM $Na_2B_4O_7$ (pH = 8.2), mobile phase B: mixture of methanol: acetonitrile: water = 45: 45: 10; gradient elution: 0-0.35 min, 2% B; 0.35-13.4 min, 2%-57% B; 13.4-13.5 min, 57%-100% B; 13.5-15.7 min, 100% B; 15.7-15.8 min, 100%−2% B; 15.8-24 min, 2% B; flow rate: 1.5 mL/min; column temperature: 40 ℃; detection wavelengths: 338 nm (bandwidth of 10 nm, reference wavelength of 390 nm, bandwidth of 20 nm) and 262 nm (bandwidth of 16 nm, reference wavelength of 324 nm, bandwidth of 8 nm). The sample injection was performed using the automatic sampler program: 1 μL of sample and 2.5 μL of borate buffer were mixed for 0.2 min. 0.5 μL of OPA solution was reacted with 0.4 μL of FMOC solution, followed by the addition of 32 μL of diluent for sample injection detection.

2.4.5 Nucleoside analysis

Control solution preparation: appropriate amounts of cytidine, uridine, guanosine, and adenine were dissolved in water to prepare control solutions with concentrations of 237.6 μg/mL, 300.0 μg/mL, 233.2 μg/mL, and 142.6 μg/mL.

Test solution preparation: approximately 0.4 g of sample powder was added with 20 mL of boiling water, and ultrasonicated in an ultrasonic cleaner for 30 min. After mixing, the supernatant was filtered through a 0.22 μm membrane to obtain the subsequent filtrate as the test solution.

Chromatographic conditions: Agilent Zorbax SB-Aq column (250 mm × 4.6 mm, 5 μm); mobile phase A: aqueous solution containing 1 mmol/L ammonium acetate and 3 mmol/L NaH_2PO_4-Na_2HPO_4 buffer (pH = 5.8), mobile phase B: methanol; gradient elution: 0-20 min, 0%-2% B; 20-35 min, 2%-20% B; 35-53 min, 20% B; 53-55 min, 20%-0% B; 55-60 min, 0% B; flow rate: 0.9 mL/min; column temperature: 25°C; injection volume: 10 μL; detection wavelength: 260 nm.

2.4.6 Sterol analysis

Control solution preparation: appropriate amounts of ergosterol, cholesterol, stigmasterol, and sitosterol were dissolved in a 0.5 mol/L potassium hydroxide-ethanol solution to prepare a mixed reference solution with concentrations of 500 μg/mL.

Test solution preparation: approximately 0.5 g of sample powder blended with 10 mL of 0.5 mol/L potassium hydroxide-ethanol solution underwent reflux in an 85 ℃ water bath for 30 min. The supernatant was filtered through a 0.45 μm membrane, and the subsequent filtrate was obtained as the test solution.

Chromatographic conditions: Waters XBridge C18 column (250 mm × 4.6 mm, 5 μm); mobile phase A: water, mobile phase B: 0.005% formic acid-methanol solution; gradient elution: 0-10 min, 97%-100% B; 10-25 min, 100% B; flow rate: 1 mL/min; column temperature: 30 ℃; injection volume: 25 μL; ELSD detector parameters: nitrogen as carrier gas; gas flow rate: 1.6 SLM; evaporation temperature: 35 ℃; nebulization temperature: 35 ℃; gain value: 6.

2.4.7 HPLC-Q-TOF analysis

Test solution preparation: approximately 0.5 g of sample powder was added with 7.5 mL of 50% methanol, and underwent sonication in an ultrasonic cleaner for 30 min. The supernatant was filtered through a 0.22 μm membrane, with the subsequent filtrate as the test solution.

Chromatographic conditions: Agilent Poroshell 120 SB-Aq column (100 mm × 4.6 mm, 2.7 μm); mobile phase A: 0.1% formic acid, mobile phase B: acetonitrile; gradient elution: 0-2 min, 0%-7.2% B; 2-5 min, 7.2% B; 5-13 min, 7.2%-9% B; 13-20 min, 9%-10% B; 20-21 min, 10%-18% B; 21-25 min, 18% B; 25-35 min, 18%-20% B; 35-45 min, 20%-22% B; 45-60 min, 22%-40% B; 60-62 min, 40%-100% B; 62-65 min, 100% B; 65-67 min, 100%-50% B; 67-70 min, 50%-0% B; flow rate: 0.6 mL/min; column temperature: 25 ℃; injection volume: 10 μL; detection wavelength: 0-24 min, 275 nm; 24-60 min, 350 nm; 60-70 min, 260 nm.

Mass spectrometry conditions: Electrospray Ionization (ESI) ion source; negative ion mode; nitrogen as carrier gas; gas flow rate of 8 L/min; dry gas temperature of 320 ℃; nebulizer pressure of 38 psi; sheath gas flow rate of 11 L/min; capillary voltage of 4000 V; collision-induced dissociation voltage of 175 V; ion scan range of 100-1000 m/z.

2.4.8 Volatile component analysis

Test sample preparation: approximately 1 g of sample powder was sealed in a 20 mL gas phase bottle.

Chromatographic conditions: Solid-phase microextraction (SPME) needle was used for extraction (50 ℃, 60 min), followed by thermal desorption for 5 min. Agilent DB-WAX UI column (30 m × 0.32 mm, 0.5 μm); carrier gas: helium; flow rate: 2 mL/min; injection port temperature: 270 ℃ with splitless mode; temperature program: 35 ℃ for 5 min; increasing to 75 ℃ at 5 ℃/min and maintaining for 5 min; increasing to 140 ℃ at 5 ℃/min; increasing to 150 ℃ at 2 ℃/min and maintaining for 5 min; increasing to 220 ℃ at 10 ℃/min and maintaining for 2 min.

Mass spectrometry conditions: Electron Ionization (EI) ion source; electron energy: 70 eV; transfer line temperature: 300 ℃; ion source temperature: 230 ℃; quadrupole temperature: 150 ℃; mass scan range: 30-500 amu.

Compounds were identified by searching against the National Institute of Standards and Technology (NIST) Mass Spectral Libraries (NIST, NIST 17).

2.4.9 Trace element analysis

Control solution preparation: appropriate amounts of each element standard solutions were pipetted to prepare a series of standard working solutions at suitable concentrations.

Test solution preparation: 0.5 g of sample powder was placed into a digestion vessel, and reacted with 6 mL of concentrated nitric acid at room temperature for 1 h. The vessel was sealed and placed in a microwave digestion system for complete digestion. Later, the digestion solution was transferred to a 50 mL volumetric flask with 0.2 mL of 1 μg/mL Au single-element standard solution, diluted to indicated scale with ultrapure water and mixed well.

Mass spectrometry conditions: parameters for the plasma, lenses, collision/reaction cell, quadrupole, and Electron-Multiplier (EM) module were optimized via automatic tuning; analysis mode: He collision mode; scanning mode: single quadrupole; acquisition mode: mass spectrum; measurement points: 3; replicates: 3; scans: 100.

The ratio (Ratio value) of the measured element's counts per second (CPS) value to the internal standard element's CPS value in the series of standard working solutions was taken as the vertical coordinate, and the concentration as the horizontal coordinate. A standard curve was plotted, and the concentration of the measured element was obtained from the standard curve.

2.4.10 Network pharmacology

2.4.10.1 Obtainment of targets

Bioactive compounds targets: The Simplified Molecular Input Line Entry System (SMILES) numbers of the compounds identified above were collected from the PubChem database (https://pubchem.ncbi.nlm.nih.gov/) and imported into the Swiss ADME database (http://www.swissadme.ch/) [23]. The criteria required "High" gastrointestinal absorption and at least two "yes" ratings among these five drug-likeness rules: Lipinski, Ghose, Veber, Egan, and Muegge [24]. Additionally, the Traditional Chinese Medicine Systems Pharmacology (TCMSP) database (https://www.tcmsp-e.com/) [25] was used to screen active components based on oral bioavailability (OB) $\geqslant$ 30% and drug-like properties (DL) $\geqslant$ 0.18 [26]. The higher content of the components in alpine bistort rhizome (arginine, Glucogallin, neochlorogenic acid, cryptochlorogenic acid, chlorogenic acid, delphinidin-3-galactoside, quercetin-5-O-glucoside, quercetin-3-O-glucuronide, 3,5-dicaffeoylquinic acid and 4,5-dicaffeoylquinic acid) was also included in the present analysis. The screened compounds were used to predict targets via the Swiss Target Prediction database (http://www.swisstargetprediction.ch/) [27]. Using probability > 0 as the screening criterion, after merging and removal of duplicates, the potential targets of the components in alpine bistort rhizome were obtained.

Diarrhea targets: With "Diarrhea" as the keyword, screening was conducted in the GeneCards (https://www.genecards.org/), Online Mendelian Inheritance in Man (OMIM) (https://omim.org/), and Therapeutic Target Database (TTD) (https://db.idrblab.net/ttd/) databases. After duplicate targets were removed, the potential targets associated with diarrhea were obtained.

The drug targets and disease targets were imported into the Venny 2.1.0 online platform (https://bioinfogp.cnb.csic.es/tools/venny/) to obtain the intersecting targets.

2.4.10.2 Construction of protein–protein interaction network

The obtained intersection targets were imported into the STRING database (https://string-db.org), with the species set as "Homo sapiens" and a minimum confidence level of 0.7, to obtain a protein–protein interaction (PPI) network diagram. The results were further visualized using the network analysis and visualization software (Cytoscape 3.10.3). Topological analysis of the network was performed, and the CytoHubba plugin's Degree algorithm was used to identify the key interacting targets.

2.4.10.3 Gene Ontology (GO) and Kyoto Encyclopedia of Genes and Genomes (KEGG) enrichment analysis

Intersecting targets were input into the Database for Annotation, Visualization, and Integrated Discovery database (DAVID) (https://davidbioinformatics.nih.gov/) to perform GO functional annotation and KEGG pathway enrichment. With P values as screening criteria, the top 10 biological processes (BP), cellular components (CC), and molecular functions (MF), as well as the top 30 signaling pathways were exported [28]. The SRplot platform (http://www.bioinformatics.com.cn/) was employed to draw a diagram.

2.4.10.4 Construction of the "herbal medicine-components-targets-pathways" network

Active ingredients, intersecting targets, and enriched pathway data were integrated to establish a network file, and the file was imported into visualization software (Cytoscape 3.10.3) to construct a "herbal medicine-components-targets-pathways" diagram.

2.4.11 Molecular docking

The molecular docking was performed on the first five core targets obtained from screening and the active ingredients. The 3D structure of drug molecules and

the crystal structure of target proteins were downloaded from the PubChem database and the Research Collaboratory for Structural Bioinformatics (RCSB) Protein Data Bank database (https://www.rcsb.org/), respectively. Molecular visualization software (PyMOL version 3.1.5.1) was used to remove water and ligands from proteins, and AutoDockTools-1.5.7 was applied to perform hydrogenation, charge calculation, and other treatments on proteins. Finally, molecular docking between the small molecule compounds and the target proteins was conducted using AutoDock Vina 1.1.2 [29]. The docking results were visualized and analyzed with Pymol.

3 Results

3.1 Molecular weight of polysaccharides

The polysaccharides extracted from alpine bistort rhizome had three major chromatographic peaks. The molecular weight ranges of peak 1, 2, and 3 were approximately 3.76×10^8 - 4.50×10^8, 5.08×10^4 - 5.53×10^4, and 980-2009 Da, respectively. Peak 4, with a molecular weight below 500 Da, may be small-molecule compounds from the sample preparation process. The predominant components of polysaccharide in the rhizome was peak 2, which accounted for over 60% of the total peak area (Figure 1, Table 2).

Table 2 Detection results of molecular weight of polysaccharides in alpine bistort rhizome.

Sample	Peak 1		Peak 2		Peak 3		Peak 4	
	Molecular weight	Percentage of peak area	Molecular weight	Percentage of peak area	Molecular weight	Percentage of peak area	Molecular weight	Percentage of peak area
S01	—	—	5.08×10^4	83.5%	1899	11.5%	101	5.0%
S02	3.76×10^8	2.2%	5.17×10^4	77.4%	2009	16.4%	155	4.0%
S03	4.50×10^8	8.1%	5.53×10^4	65.0%	980	26.9%	—	—

Note: — Not detected.

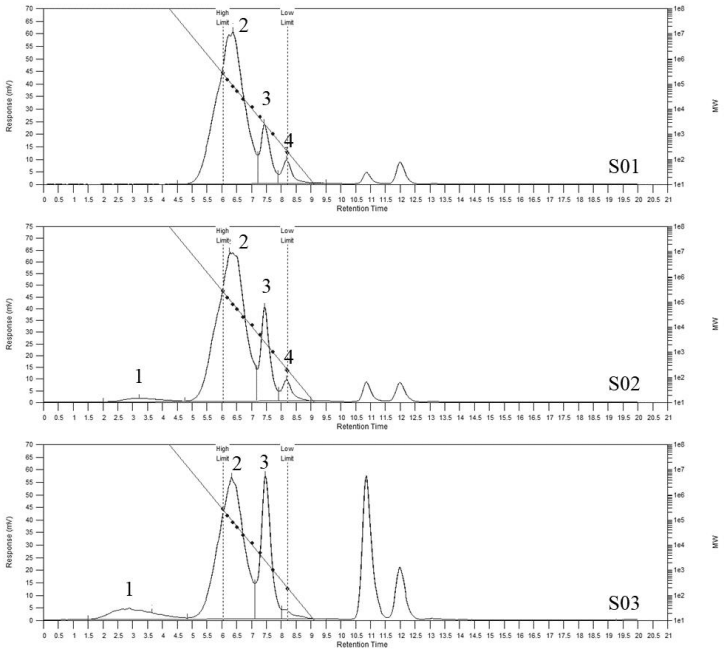

Figure 1 Chromatogram of polysaccharide molecular weight of the samples of alpine bistort rhizome.

3.2 Monosaccharide components of polysaccharides

The molar ratios of other monosaccharide components were calculated with the measured quantity of glucose as 1. The results indicated that the polysaccharides in alpine bistort rhizome were rich in glucose, galactose, and arabinose, with glucose being the most abundant (Figure 2, Table 3), consistent with the findings of Man et al [30]. It was speculated that the polysaccharides in the rhizome may primarily consist of starch, which provided energy support and promoted the growth of alpine bistort.

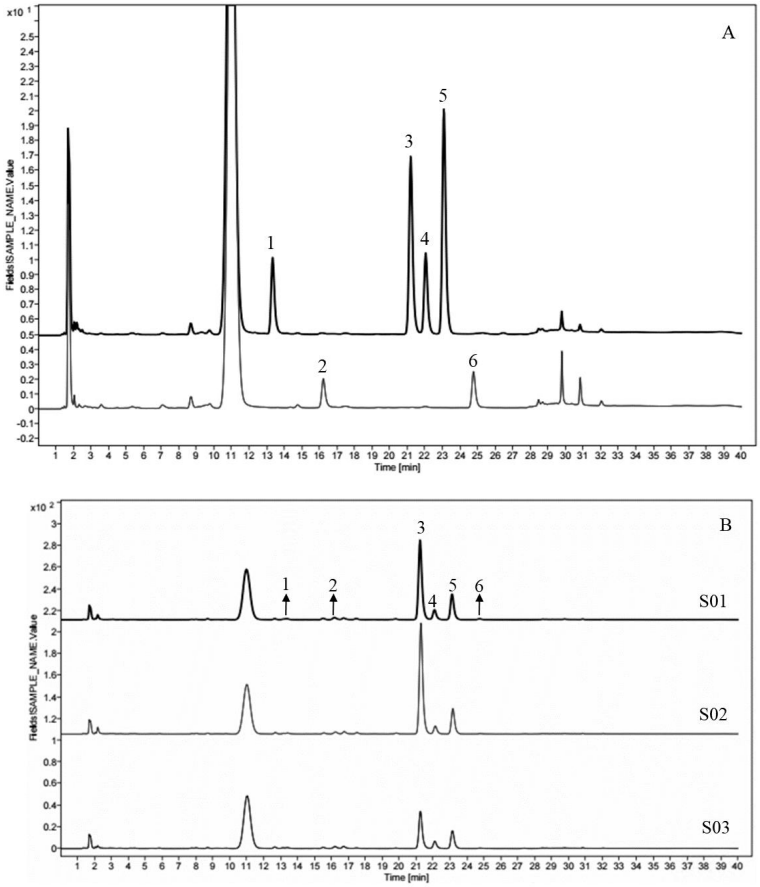

Figure 2 Monosaccharide components chromatograms of polysaccharides of controls (A) and alpine bistort rhizome samples (B). 1: Mannose; 2: Rhamnose; 3: Glucose; 4: Galactose; 5: Arabinose; 6: Fucose.

Table 3 Molar ratios of monosaccharide components and polysaccharides in alpine bistort rhizome.

Sample	Mannose	Rhamnose	Glucose	Galactose	Arabinose	Fucose
S01	0.02	0.03	1.00	0.11	0.31	0.01
S02	0.01	0.02	1.00	0.06	0.22	0.00
S03	0.02	0.07	1.00	0.17	0.46	0.01

3.3 Free sugar analysis

Fructose, glucose, and sucrose were detected in three batches of alpine bistort rhizome samples in this experiment (Figure 3). Among them, the peak areas of sucrose in batches S01 and S02 were the highest, exceeding 50%. The peak areas of fructose and glucose were similar. The free sugar content in batch S03 was lower, with comparable peak areas for fructose, glucose, and sucrose.

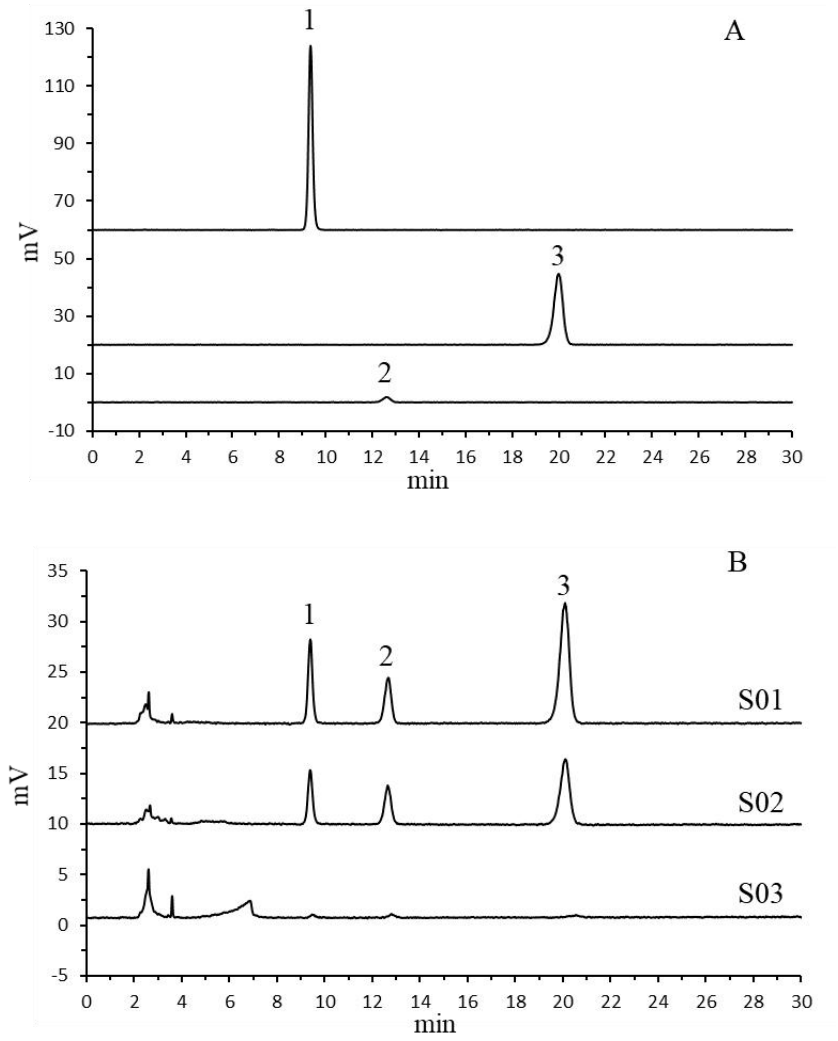

Figure 3 Free sugar chromatograms of controls (A) and alpine bistort rhizome samples (B). 1: Fructose; 2: Glucose; 3: Sucrose.

3.4 Amino acid analysis

The chromatograms of amino acid detection (Figures 4-5) revealed the presence of 16 free amino acids in alpine bistort rhizome, including glutamic acid, asparagine, serine, glutamine, histidine, glycine, threonine, arginine, alanine, tyrosine, valine, tryptophan, phenylalanine, isoleucine, leucine, and lysine. Among them, there were seven essential amino acids: lysine, tryptophan, phenylalanine, threonine, isoleucine, leucine, and valine. Asparagine, glutamine, and tryptophan were not detected in the hydrolyzed amino acids of the rhizomes, but aspartic acid was identified.

The arginine content was the highest among the three batches of samples, all exceeding 1%. This distribution may be related to arginine as an important form of nitrogen storage in plants, which is widely present in seeds and rhizomes. Additionally, under adverse conditions such as saline-alkali and drought, plants may enhance their stress resistance by increasing arginine synthesis, which positively facilitated the growth of alpine bistort in plateau regions.

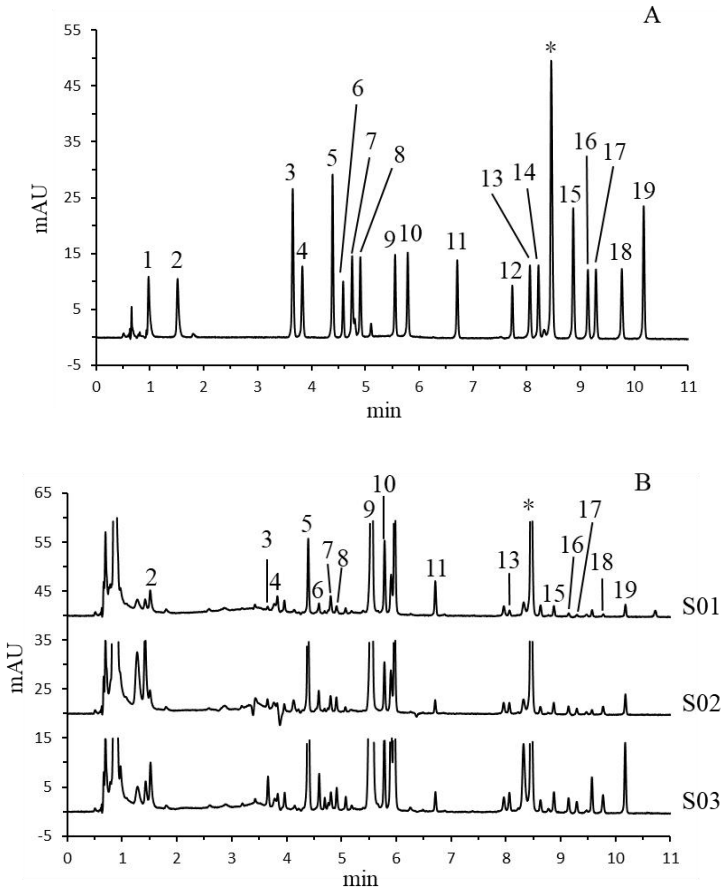

Figure 4 Chromatograms of free amino acids in controls (A) and alpine bistort rhizome samples (B). 1: Aspartic acid; 2: Glutamic acid; 3: Asparagine; 4: Serine; 5: Glutamine; 6: Histidine; 7: Glycine; 8: Threonine; 9: Arginine; 10: Alanine; 11: Tyrosine; 12: Cystine; 13: Valine; 14: Methionine; 15: Tryptophan; 16: Phenylalanine; 17: Isoleucine; 18: Leucine; 19: Lysine; * Internal standard.

3.5 Nucleoside analysis

The results of nucleoside analysis indicated that alpine bistort rhizome contained three types of nucleosides, including uridine, guanosine, and adenine (Figure 6).

3.6 Sterol analysis

The sterol analysis results implied that alpine bistort rhizome consisted of sitosterol and stigmasterol, with sitosterol as the major sterol compound. Stigmasterol was a newly-discovered component in this plant (Figure 7).

3.7 HPLC-Q-TOF analysis

HPLC-Q-TOF was employed to dissect the chemical constituents in alpine bistort rhizome. Based on retention times of controls, accurate molecular masses and major fragment ions, a total of 40 chemical components were identified in the rhizomes (Table 4), including 2 amino acids, 14 organic acids, 21 flavonoids, 2 glycosides, and 1 sugar-conjugated polymer. Among them, 3 organic acids (protocatechuic acid, 4-O-p-coumaroylquinic acid, 3-O-p-coumaroylquinic acid), 9 flavonoids (protocatechuic, catechin-5-O-glucoside, delphinidin-3-galactoside, eriodictyol-7-O-glucoside, protocatechuic B_2-3-O-gallate, protocatechuic B_3-3-O-gallate, quercetin-5-O-glucoside, quercetin-7-O-rutinoside, 3,4-dicaffeoylquinic acid), 1 glycoside (pleoside), and 1 sugar-conjugated polymer ((2S,3S,4S,5R,6R)-6-(3-Benzoyloxy-2-hydroxypropoxy)-3,4,5-trihydroxyoxane-2-carboxylic acid) were reported for the first time.

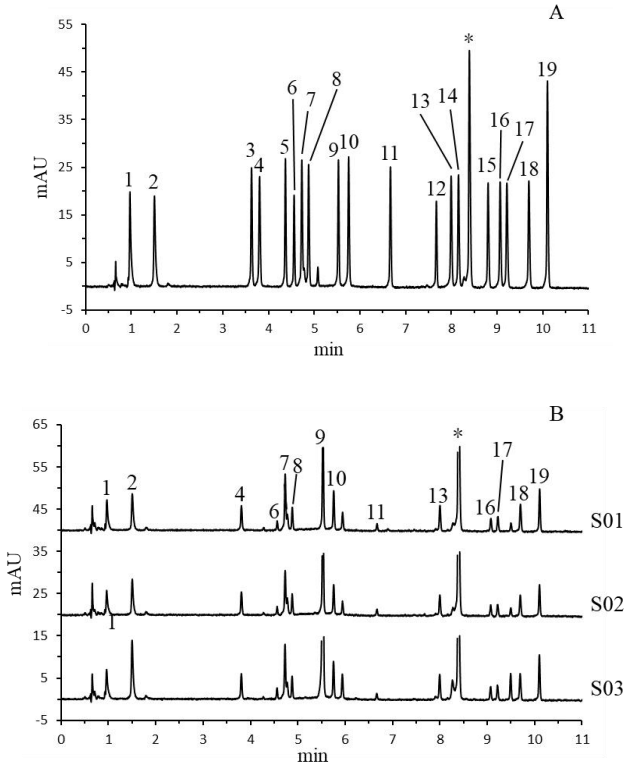

Figure 5 Chromatograms of hydrolyzed amino acids in controls (A) and alpine bistort rhizome samples (B). 1: Aspartic acid; 2: Glutamic acid; 3: Asparagine; 4: Serine; 5: Glutamine; 6: Histidine; 7: Glycine; 8: Threonine; 9: Arginine; 10: Alanine; 11: Tyrosine; 12: Cystine; 13: Valine; 14: Methionine; 15: Tryptophan; 16: Phenylalanine; 17: Isoleucine; 18: Leucine; 19: Lysine; * Internal standard.

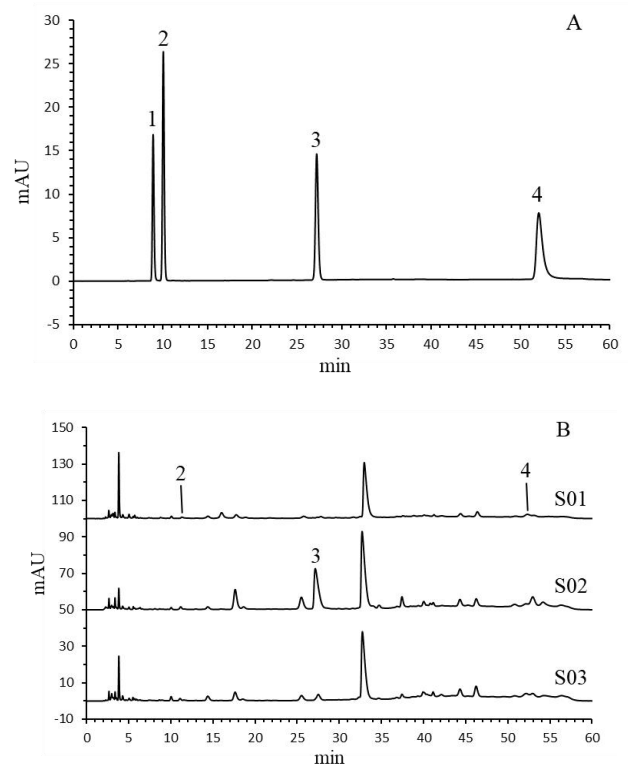

Figure 6 Chromatograms of nucleosides in controls (A) and alpine bistort rhizome samples (B). 1: Cytidine; 2: Uridine; 3: Guanosine; 4: Adenine

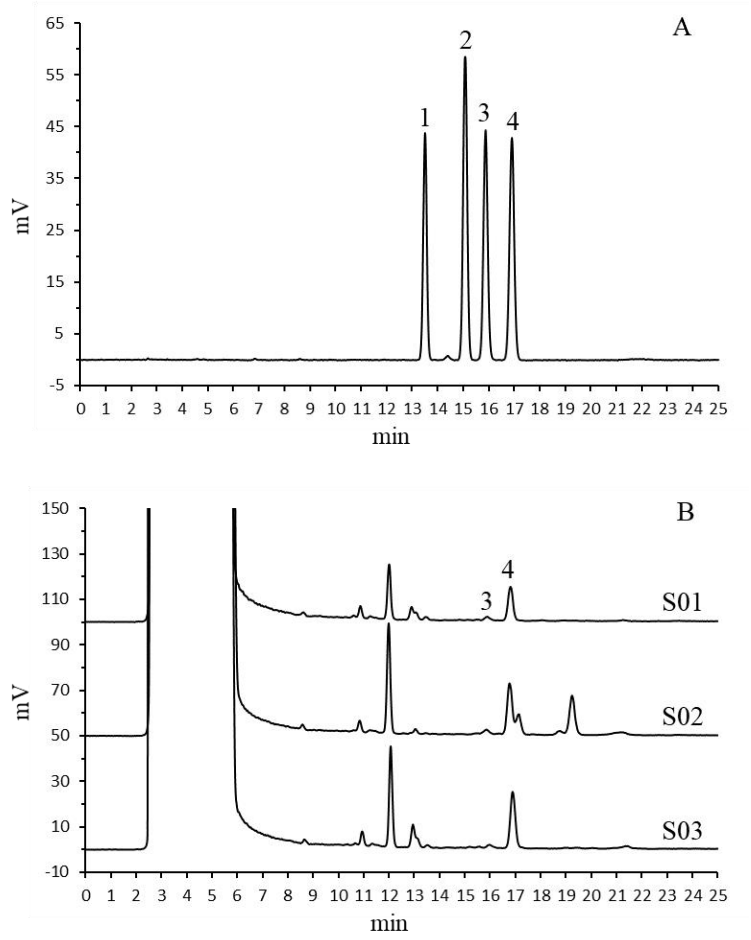

Figure 7 Chromatograms of sterols in controls (A) and alpine bistort rhizome samples (B). 1: Ergosterol; 2: Cholesterol; 3: Stigmasterol; 4: Sitosterol.

Table 4 Mass spectrometry identification results of components of alpine bistort rhizome.

Number of peaks	t_R (min)	Compound name	Molecular formula	Precise molecular weight	Theoretical value (m/z)	Quasi-molecular ion (m/z)	Type of ion	Deviation (ppm)	Fragment ion(m/z)	Type of compounds
1	1.96	Arginine	$C_6H_{14}N_4O_2$	174.1262	175.1196	175.1198	$[M+H]^+$	1.11	158.0921, 130.0970, 116.0703, 70.0652, 60.0551	Amino acid
2	2.36	Quinic acid	$C_7H_{12}O_6$	192.0634	191.0556	191.0556	$[M-H]^-$	0.18	173.0451, 127.0398, 93.0343, 59.0135, 50.0290	Organic acid
3	3.03	Citric acid	$C_6H_8O_7$	192.0270	191.0192	191.0189	$[M-H]^-$	-1.47	111.0146, 87.0132, 85.0338, 57.0373	Organic acid
4	3.63	Phenylalanine	$C_9H_{11}NO_2$	165.0790	166.0868	166.0859	$[M+H]^+$	-5.6	120.0799, 103.0539, 91.0539, 77.0382	Amino acid
5	5.85	Gallic acid	$C_7H_6O_5$	170.0215	169.0137	169.0140	$[M-H]^-$	1.77	125.0243, 97.0295, 79.0188, 51.0238	Organic acid
6	6.24	Glucogallin	$C_{13}H_{16}O_{10}$	332.0744	331.0665	331.0670	$[M-H]^-$	1.43	271.0468, 211.0256, 169.0147, 124.0168	Glucoside
7	6.85	Procyanidin trimer isomer	$C_{45}H_{38}O_{18}$	866.2058	865.1980	865.1970	$[M-H]^-$	-1.15	407.0785, 243.0305, 289.0727, 125.0244	Flavone

8	7.46	Protocatechuic acid	$C_7H_6O_4$	154.0266	153.0188	153.0184	$[M-H]^-$	-2.52	109.0284, 81.0340, 65.0024	Organic acid
9	8.79	Procyanidin	$C_{30}H_{26}O_{13}$	594.1373	593.1295	593.1300	$[M-H]^-$	0.81	407.0780, 289.0723, 177.0196, 125.0243	Flavone
10	9.24	Catechin-5-O-glucoside	$C_{21}H_{24}O_{11}$	452.1319	451.1240	451.1238	$[M-H]^-$	-0.53	289.0720, 203.0715, 245.0821, 137.0242, 109.0295	Flavone
11	9.75	Neochlorogenic acid	$C_{16}H_{18}O_9$	354.0951	353.0873	353.0876	$[M-H]^-$	0.96	191.0557, 179.0347, 161.0238, 135.0448	Organic acid
12	10.89	Syringic acid	$C_9H_{10}O_5$	198.0528	199.0607	199.0598	$[M+H]^+$	-4.27	181.0804, 155.0656, 140.0425, 123.0400, 95.0459, 77.0360	Organic acid
13	12.98	4-O-p-Coumaroylquinic acid	$C_{16}H_{18}O_8$	338.1002	337.0923	337.0920	$[M-H]^-$	-1.03	191.0452, 163.0310, 119.0434, 93.0292	Organic acid
14	13.07	3-O-p-coumaroylquinic acid	$C_{16}H_{18}O_8$	338.1002	337.0923	337.0920	$[M-H]^-$	-1.03	179.0572, 119.0356, 101.0255, 89.0247	Organic acid
15	14.48	Procyanidin trimer isomer	$C_{30}H_{26}O_{12}$	578.1424	577.1346	577.1346	$[M-H]^-$	-0.01	451.1049, 407.0786, 289.0727, 161.0246, 125.0246	Flavone
16	15.05	Catechin	$C_{15}H_{14}O_6$	290.0790	289.0712	289.0713	$[M-H]^-$	0.29	151.0398, 125.0243, 123.0452, 109.0295, 97.0295	Flavone
17	15.18	(2S,3S,4S,5R,6R)-6-(3-Benzoyloxy-2-hydroxypropoxy)-3,4,5-trihydroxyoxane-2-carboxylic acid	$C_{16}H_{20}O_{10}$	372.1057	371.0978	371.0972	$[M-H]^-$	-1.69	249.0620, 121.0299, 59.0137	Sugar-conjugated polymer
18	15.85	Cryptochlorogenic acid	$C_{16}H_{18}O_9$	354.0951	353.0873	353.0876	$[M-H]^-$	0.96	191.0566, 179.0355, 173.0460, 135.0454	Organic acid
19	15.93	Caffeic acid	$C_9H_8O_4$	180.0423	179.0344	179.0348	$[M-H]^-$	2.04	135.0453, 107.0495, 79.0552	Organic acid
20	16.89	Chlorogenic acid	$C_{16}H_{18}O_9$	354.0951	353.0873	353.0876	$[M-H]^-$	0.96	191.0563, 179.0350, 161.0243, 135.0453	Organic acid
21	17.44	Delphinidin-3-galactoside	$C_{21}H_{21}O_{12}^+$	465.1033	465.1033	465.1029	$[M]^+$	-0.87	303.0515, 285.0405, 125.0241	Flavone
22	19.12	Procyanidin dimer isomers	$C_{30}H_{26}O_{12}$	578.1424	577.1346	577.1346	$[M-H]^-$	-0.01	425.0903, 407.0798, 289.0734, 125.0247	Flavone
23	19.60	Eriodictyol-7-O-glucoside	$C_{21}H_{22}O_{11}$	450.1162	449.1084	449.1075	$[M-H]^-$	-1.98	287.0567, 259.0610, 151.0012, 125.0242	Flavone

24	20.22	Epicatechin	$C_{15}H_{14}O_6$	290.0790	289.0712	289.0713	$[M-H]^-$	0.29	289.0722, 245.0820, 203.0716, 123.0453, 109.0296, 97.0295	Flavone
25	21.00	Procyanidin trimer isomer	$C_{45}H_{38}O_{18}$	866.2058	865.1980	865.1970	$[M-H]^-$	-1.15	577.1367, 407.0780, 289.0725, 125.0246	Flavone
26	25.02	Procyanidin trimer isomer	$C_{45}H_{38}O_{18}$	866.2058	865.1980	865.1970	$[M-H]^-$	-1.15	577.1367, 425.0890, 287.0566, 125.0244	Flavone
27	25.12	Pleoside	$C_{15}H_{20}O_9$	344.1107	345.1186	345.1179	$[M+H]^+$	-1.92	183.0651, 165.0542, 137.0593, 119.0488	Glucoside
28	26.09	Procyanidin dimer isomers	$C_{30}H_{26}O_{12}$	578.1424	577.1346	577.1336	$[M-H]^-$	-1.74	407.0774, 289.0721, 245.0818, 161.0240, 125.0241	Flavone
29	26.45	Procyanidin B_2-3-O-gallate	$C_{37}H_{30}O_{16}$	730.1534	729.1456	729.1445	$[M-H]^-$	-1.46	577.1356, 407.0768, 289.0717, 125.0240	Flavone
30	27.18	Procyanidin B_3-3-O-gallate	$C_{37}H_{30}O_{16}$	730.1534	729.1456	729.1445	$[M-H]^-$	-1.46	577.1367, 407.0780, 289.0720, 125.0243	Flavone
31	28.70	Quercetin-5-O-glucoside	$C_{21}H_{20}O_{12}$	464.0955	463.0877	463.0870	$[M-H]^-$	-1.42	301.0359, 255.0301, 151.0037	Flavone
32	29.21	Quercetin-7-O-rutinoside	$C_{27}H_{30}O_{16}$	610.1534	609.1456	609.1452	$[M-H]^-$	-0.60	463.0858, 301.0347, 300.0280, 151.0037	Flavone
33	29.81	Rutin	$C_{27}H_{30}O_{16}$	610.1534	609.1456	609.1459	$[M-H]^-$	0.55	301.0336, 300.0272, 271.0246, 151.0033	Flavone
34	30.55	Isoquercitrin	$C_{21}H_{20}O_{12}$	464.0955	463.0877	463.0870	$[M-H]^-$	-1.42	300.0273, 271.0247, 255.0295, 178.9976, 151.0034	Flavone
35	31.12	Hyperoside	$C_{21}H_{20}O_{12}$	464.0955	463.0877	463.0870	$[M-H]^-$	-1.42	301.0327, 300.0278, 271.0244, 255.0295	Flavone
36	31.69	Quercetin-3-O-glucuronide	$C_{21}H_{18}O_{13}$	478.0747	477.0669	477.0671	$[M-H]^-$	0.38	301.0038, 150.9860	Flavone
37	34.55	3,4-dicaffeoylquinic acid	$C_{25}H_{24}O_{12}$	516.1268	515.1190	515.1181	$[M-H]^-$	-1.66	353.0869, 191.0551, 179.0341, 173.0448, 135.0442	Organic acid
38	35.84	Quercetin-4'-O-glucoside	$C_{21}H_{20}O_{12}$	464.0955	465.1033	465.1024	$[M+H]^+$	-1.95	303.0494, 229.0491, 85.0279	Flavone
39	36.83	3,5-dicaffeoylquinic acid	$C_{25}H_{24}O_{12}$	516.1268	515.1190	515.1181	$[M-H]^-$	-1.66	353.0889, 191.0560, 179.0352, 173.0453, 135.0449	Organic acid
40	39.57	4,5-dicaffeoylquinic acid	$C_{25}H_{24}O_{12}$	516.1268	515.1190	515.1181	$[M-H]^-$	-1.66	353.0873, 191.0555, 179.0347, 173.0451, 135.0447	Organic acid

3.8 Volatile component analysis

The volatile components identified in alpine bistort rhizome were listed in Table 5. By comparing with the NIST standard mass spectral library, 34 components were detected in the rhizome samples. With the exception of citronellol, all other volatile components were identified for the first time from alpine bistort rhizome.

Table 5 Identification results of volatile components in alpine bistort rhizome.

Number of peaks	t_R (min)	Compound name	Molecular formula
1	5.866	Ethanol	C_2H_6O
2	9.359	Decane, 2-methyl-	$C_{11}H_{24}$
3	9.704	Decane, 3-methyl-	$C_{11}H_{24}$
4	10.447	Hexanal	$C_6H_{12}O$
5	10.684	Undecane	$C_{11}H_{24}$
6	14.085	Dodecane	$C_{12}H_{26}$
7	15.115	2-Hexanal	$C_6H_{10}O$
8	15.685	Furan, 2-pentyl-	$C_9H_{14}O$
9	16.905	1-Pentanol	$C_5H_{12}O$
10	18.490	Acetoin	$C_4H_8O_2$
11	20.520	2-Heptanol	$C_7H_{16}O$
12	21.002	5-Hepten-2-one, 6-methyl-	$C_8H_{14}O$
13	21.904	1-Hexanol	$C_6H_{14}O$
14	23.182	Nonanal	$C_9H_{18}O$
15	23.719	3-Octen-2-one	$C_8H_{14}O$
16	24.448	2-Octenal, (E)-	$C_8H_{14}O$
17	25.055	Acetic acid	$C_2H_4O_2$
18	25.366	1-Octen-3-ol	$C_8H_{16}O$
19	27.476	2-Nonanol	$C_9H_{20}O$
20	28.099	2,3-Butanediol	$C_4H_{10}O_2$
21	28.230	Linalool	$C_{10}H_{18}O$
22	29.383	Caryophyllene	$C_{15}H_{24}$
23	29.657	Cyclohexanol, 2,6-dimethyl-dimethy-	$C_8H_{16}O$
24	30.096	1-Cyclohexene, 1-carboxaldehyde, 2,6,6-trimethyl-	$C_{10}H_{16}O$
25	31.346	Butanoic acid, 3-methyl-	$C_5H_{10}O_2$
26	32.143	2-Cyclohexene-1-methanol, 2,6,6-trimethyl-	$C_{10}H_{18}O$
27	33.127	Pentanoic acid	$C_5H_{10}O_2$
28	33.866	Oxime-, methoxy-phenyl-_	$C_8H_9NO_2$
29	34.009	Citronellol	$C_{10}H_{20}O$
30	36.276	Hexanioc acid	$C_6H_{12}O_2$
31	38.682	Phenylethyl alcohol	$C_8H_{10}O$
32	39.720	3-Buten-2-one, 4-(2,6,6-trimethyl-1-cyclohexen-1-yl)-	$C_{13}H_{20}O$
33	40.513	3-Hexenoic acid, (E)-	$C_6H_{10}O_2$
34	41.957	3-Buten-2-one, 4-(2,2,6-trimethyl-7-oxabicyclo[4.1.0] hept-1-yl)-	$C_{13}H_{20}O_2$

3.9 Trace element analysis

The trace elements and their contents detected in alpine bistort rhizome were listed in Table 6. A total of 19 elements were detected, with 10 essential trace elements for the human body (Se, Fe, Zn, Mn, Co, Mo, Sn, Cr, Cu, Ni) and 4 essential macroelements for the human body (Na, Mg, K, Ca). The contents of iron, magnesium, potassium, and calcium were relatively high in the rhizomes. The contents of elements harmful to humans, such as arsenic, lead, mercury, cadmium, and chromium, were low.

Table 6 Detection results of trace element content in alpine bistort rhizome (mg/kg).

Elements	S01	S02	S03
As	0.1	0.08	0.1
Pb	1.0	2.7	0.5
Hg	< 0.02	< 0.02	< 0.02
Cd	1.6	0.5	1.5
Cr	0.5	0.2	0.3
Cu	3.3	6.0	4.3
Ni	2.5	4.5	5.0
Se	0.1	0.2	0.4
Na	23.2	85.6	31.3
Fe	217.5	133.7	123.8
Zn	27.4	38.6	28.0
Mg	1338.4	2374.3	1431.0
Al	471.8	577.6	440.5
K	7664.9	6198.9	11868.3
Ca	20680.7	29969.1	35706.2
Mn	77.5	62.8	139.4
Co	0.6	0.8	0.6
Mo	0.08	0.07	0.3
Sn	< 0.03	< 0.03	< 0.03

3.10 Network pharmacology

3.10.1 Target acquisition

Based on the chemical composition analysis of the alpine bistort rhizome, a total of 63 chemical compounds were screened. SMILES numbers of 63 active components were imported into the Swiss target prediction database, and 50 components were

identified as capable of predicting targets (Table 7), a total of 441 active compound targets were identified. Using "Diarrhea" as the keyword, searches were conducted in the GeneCards, OMIM, and TTD databases. After merging and removal of duplicates, 4195 diarrhea-related targets were obtained. Venn diagram analysis of the bioactive compound targets and diarrhea targets identified 227 overlapping effect targets (Figure 8).

Table 7 Basic information of 50 chemical compounds.

Number	Compound name	CAS No.
C1	Glutamine	56-85-9
C2	Histidine	71-00-1
C3	Arginine	74-79-3
C4	Tyrosine	60-18-4
C5	Valine	72-18-4
C6	Tryptophan	73-22-3
C7	Phenylalanine	63-91-2
C8	Isoleucine	73-32-5
C9	Leucine	61-90-5
C10	Lysine	56-87-1
C11	Adenine	73-24-5
C12	Sitosterol	83-46-5
C13	Stigmasterol	83-48-7
C14	Gallic acid	149-91-7
C15	Glucogallin	58511-73-2
C16	Protocatechuic acid	99-50-3
C17	Neochlorogenic acid	906-33-2
C18	Syringic acid	530-57-4
C19	Cryptochlorogenic acid	905-99-7
C20	Caffeic acid	501-16-6
C21	Chlorogenic acid	327-97-9
C22	Delphinidin-3-galactoside	68852-84-6
C23	Quercetin-5-glucoside	34199-21-8
C24	Quercetin-3-O-glucuronide	22688-79-5
C25	Isochlorogenic acid A	2450-53-5
C26	Isochlorogenic acid C	57378-72-0
C27	Hexanal	66-25-1
C28	2-Hexanal	591-78-6
C29	Furan, 2-pentyl-	3777-69-3
C30	1-Pentanol	71-41-0
C31	2-Heptanol	543-49-7
C32	5-Hepten-2-one, 6-methyl-	110-93-0
C33	1-Hexanol	111-27-3
C34	Nonanal	124-19-6
C35	3-Octen-2-one	1669-44-9
C36	2-Octenal, (E)-	2548-87-0
C37	1-Octen-3-ol	3391-86-4

C38	2-Nonanol	628-99-9
C39	2,3-Butanediol	513-85-9
C40	Linalool	78-70-6
C41	Cyclohexanol, 2,6-dimethy-	5337-72-4
C42	1-Cyclohexene, 1-carboxaldehyde, 2,6,6-trimethyl-	432-25-7
C43	2-Cyclohexene-1-methanol, 2,6,6-trimethyl-	6627-74-3
C44	Pentanoic acid	109-52-4
C45	Citronellol	106-22-9
C46	Hexanioc acid	142-62-1
C47	Phenylethyl alcohol	1960/12/8
C48	3-Buten-2-one, 4-(2,6,6-trimethyl-1-cyclohexen-1-yl)-	79-77-6
C49	3-Hexenoic acid, (E)-	1577-18-0
C50	3-Buten-2-one, 4-(2,2,6-trimethyl-7-oxabicyclo [4.1.0] hept-1-yl)-	23267-57-4

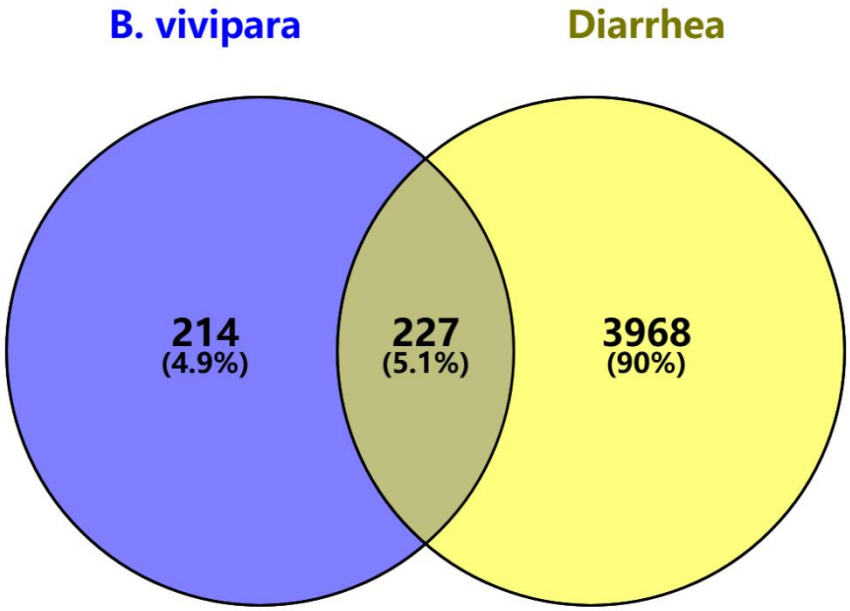

Figure 8 Venn diagram of alpine bistort rhizome components and diarrhea targets.

3.10.2 Construction of protein – protein interaction network and identification of core targets

227 intersecting targets were imported into the STRING database to obtain protein–protein interaction network. The results were input into Cytoscape 3.10.3 for further visualization (Figure 9 A). The network had a total of 211 nodes and 965 edges, with darker colors and higher degree values indicating stronger protein interactions. With the CytoHubba plugin, the top 10 targets by degree value were identified as core targets for the antidiarrheal effects of alpine bistort rhizome (Figure 9 B): Signal Transducer and Activator of Transcription 3 (STAT3), Epidermal Growth Factor Receptor (EGFR), Tumor Necrosis Factor (TNF), Heat shock protein 90kDa alpha (cytosolic), class A member 1 (HSP90AA1), Recombinant Caspase 3 (CASP3), Toll-like receptor 4 (TLR4), Albumin (ALB), Prostaglandin-Endoperoxide Synthase 2 (PTGS2), Estrogen Receptor 1 (ESR1), and Mitogen-Activated protein kinase 1 (MAPK1).

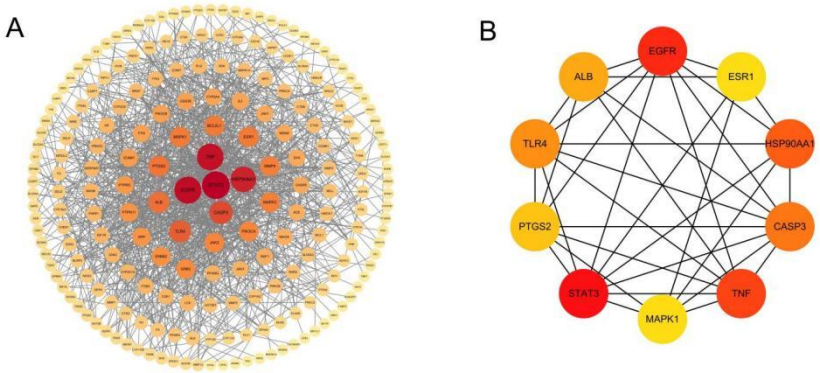

Figure 9 Protein–protein interaction network and core subnetwork. (A) Protein–protein interaction network; (B) Core subnetwork.

3.10.3 GO functional enrichment and KEGG pathway analysis

Gene Ontology and Kyoto Encyclopedia of Genes and Genomes enrichment analyses were conducted on 227 effect targets to elucidate their biological roles and associated pathways. The Gene Ontology enrichment analysis revealed that these targets are predominantly involved in biological processes such as response to exnobiotic stimulus, cellular response to amyloid-beita and response to lipopolysaccharide. Regarding cellular components, the targets are primarily associated with structures such as the plasma membrane, cytosol and membrane raft. In terms of molecular functions, the targets exhibit activities such as nuclear receptor activity, enzyme binding and heme binding (Figure 10). KEGG enrichment results revealed that the anti-diarrhea effect of alpine bistort rhizome mainly involved lipid and atherosclerosis, Advanced Glycation End products-Receptor for Advanced Glycation End products (AGE-RAGE) signaling pathway in diabetic complications, Hypoxia-Inducible Factor-1 (HIF-1), TNF signaling pathway and Phosphoinositide 3-Kinase-Protein Kinase B (PI3K-Akt) signaling pathway (Figure 11).

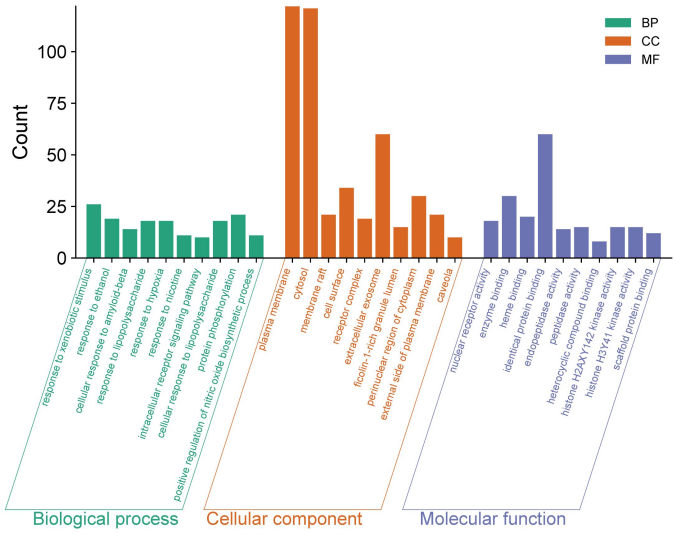

Figure 10 GO enrichment analysis.

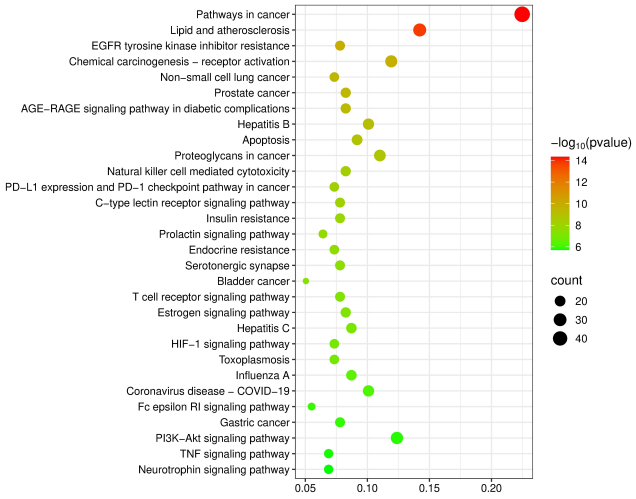

Figure 11 KEGG enrichment analysis.

3.10.4 Construction and analysis of the "herbal medicine-components-targets-pathways" network

To deeply investigate the interactions between components, targets and pathways, the top 30 significantly enriched signaling pathways and corresponding target information were selected to construct a "component-target-pathway" network using Cytoscape 3.10.3 (Figure 12). This network consisted of 309 nodes and 1,400 edges. Topological analysis of the network unveiled that the active components with the highest degree values included 2-nonanol, sitosterol, stigmasterol, caffeic acid, and isochlorogenic acid C, hinting that these might be the core compounds responsible for the antidiarrheal effects of alpine bistort rhizome. Moreover, as shown in Figure 12, the active components of alpine bistort rhizome exerted their effects by acting on multiple targets and pathways, with intricate relationships among the components, targets, and pathways.

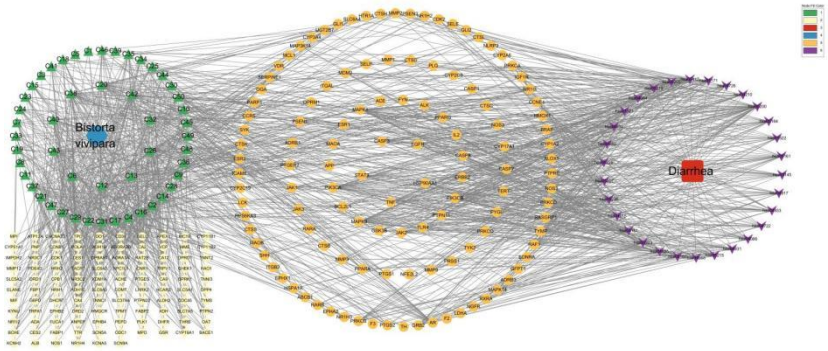

Figure 12 "Herbal medicine-components-targets-pathways" network. 1: Green triangles indicate chemical components; 2: Yellow ellipses represent compound targets unrelated to diarrhea; 3: Red squares denote diarrhea; 4: Blue hexagons represent the rhizome of alpine bistort; 5: Orange ellipses indicate the anti-diarrheal target of the rhizome of alpine bistort; 6: Purple V-shaped symbols represent the KEGG pathway.

3.11 Molecular docking

The five core targets (STAT3, EGFR, TNF, HSP90AA1, and CASP3) of alpine bistort rhizome for inhibiting diarrhea were molecularly docked with the core components. Generally, a binding energy between ligand and receptor less than 0 indicates spontaneous binding, while a binding energy below-5.0 kJ/mol suggests favorable binding activity. A binding energy of -7.0 kJ/mol is presumed to indicate strong binding activity between the compound and the target. As described in Table 8, the lowest binding energy of each target protein with the compound was less than 0, indicating that the components of alpine bistort rhizome had a strong affinity for the core targets. Further, the docking results with the lowest binding energy were visualized using PyMOL. The compounds could bind to different amino acid residues in the target through hydrogen bonds (Figure 13), thereby exerting anti-diarrhea effects.

Table 8 Molecular docking results.

Chemical compounds	Binding energy (kcal·mol^{-1})				
	EGFR	TNF	HSP90AA1	STAT3	CASP3
Sitosterol	-8.4	-6.4	-9.6	-7.2	-7.6
Stigmasterol	-8.9	-6.5	-10.1	-7.5	-8.2
Caffeic acid	-6.3	-6.0	-7.3	-6.1	-5.5
Isochlorogenic acid C	-9.1	-6.4	-9.6	-7.3	-7.6
2-nonanol	-4.9	-4.1	-5.9	-3.9	-4.7

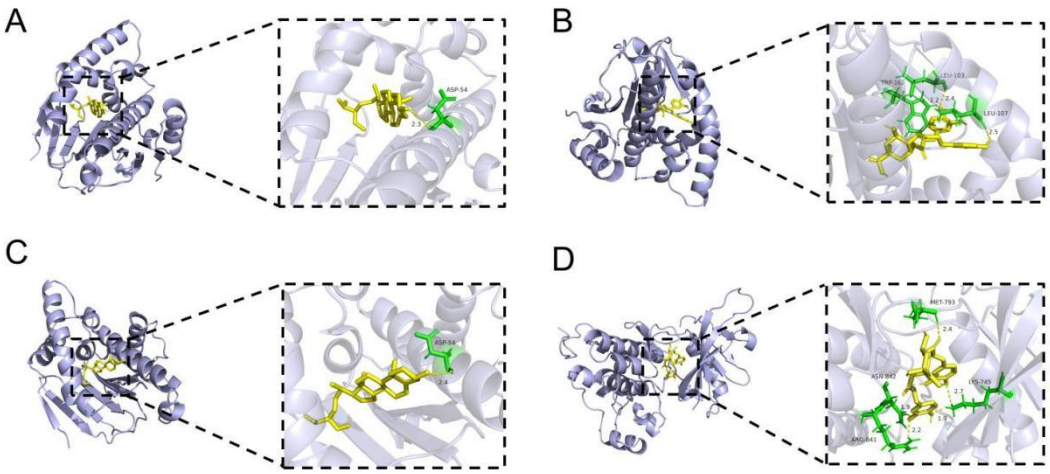

Figure 13 Visualization results of molecular docking. (A) Sitosterol-HSP90AA1; (B) Isochlorogenic acid C-HSP90AA1; (C) Stigmasterol-HSP90AA1; D: Isochlorogenic acid C-EGFR).

4 Discussion

This study conducted a systematic analysis of the chemical constituents in the rhizomes of alpine bistort from three regions: Sichuan, Yunnan, and Guizhou. A total of 126 chemical compounds were identified. The

results demonstrated that the rhizomes contain various organic acids, flavonoids, amino acid compounds, and trace elements, which are consistent with previous research reports [8,31,32]. Additionally, the study revealed the presence of polysaccharides, sterols, and volatile components in the rhizomes. These components may serve as the material basis for the pharmacological effects of alpine bistort. It is worth noting that alpine bistort is also distributed in regions such as Qinghai and Xizang, and there may be certain differences in its composition among different production areas [33]. In future studies, it is necessary to further expand the sample coverage to ensure the reliability of the research results.

The occurrence of diarrhea is often associated with factors such as intestinal inflammation, intestinal mucosal damage, and dysbiosis of the gut microbiota [34,35], making it one of the most common digestive tract diseases in China. In the "Herbal medicine-components-targets-pathways" network, 2-nonanol, sitosterol, stigmasterol, caffeic acid, and isochlorogenic acid C are highly connected compounds, serving as key active components in the network. 2-nonanol is a plant-derived antimicrobial agent with notable bacteriostatic effects [36]. Both sitosterol and stigmasterol belong to the sterol class of compounds, exhibiting anti-inflammatory and antibacterial properties [37]. β-Stigmasterol inhibits the release of inflammatory factors such as TNF-α and IL-6, thereby preventing intestinal mucosal damage [38]. Caffeic acid and isochlorogenic acid C are polyphenolic compounds that play a crucial role in enhancing intestinal barrier integrity and alleviating oxidative stress-induced intestinal damage [39,40].

PPI network analysis identified STAT3, EGFR, TNF, HSP90AA1, and CASP3 as key targets in the treatment of diarrhea by alpine bistort rhizome. STAT3, as a downstream response factor of the inflammatory cytokine IL-6, can be activated by IL-6 and participates in regulating the intestinal cell cycle progression and apoptosis, modulating the activation of intestinal immune cells [41]. EGFR is involved in cell growth, migration, and apoptosis, and serves as a growth factor in the intestinal mucosal repair process, participating in the regulation of intestinal mucosal injury. It also plays a significant role in regulating Cl-secretion in both normal and inflammatory colons [42,43]. Studies have found that the inflammatory cytokine TNF-α can affect gastrointestinal motility, secretion, and reabsorption, and increase intestinal sensitivity in patients with diarrhea [44]. As a key apoptosis execution protein, CASP3 plays a central role in regulating apoptosis [45]. HSP90AA1, a heat shock protein, enhances ischemia-reperfusion-induced necrotic apoptosis in the intestine by participating in the expression of Phosphorylated Mixed Lineage Kinase Domain-Like Protein (p-MLKL) [46].

KEGG enrichment analysis revealed that lipid and atherosclerosis, the AGE-RAGE signaling pathway in diabetic complications, HIF-1 signaling pathway, TNF signaling pathway, and PI3K-Akt signaling pathway may serve as the primary mechanisms underlying the therapeutic effects of alpine bistort rhizome in treating diarrhea. Multiple studies have demonstrated a significant association between lipid metabolism and gastrointestinal diseases. Restoring normal intestinal physiological functions can be achieved by regulating genes related to lipid metabolism [47-49]. The AGE-RAGE signaling pathway activates various intracellular signaling pathways, including NADPH oxidase and protein kinase C, thereby inducing nuclear factor kappa-B (NF-κB) activity [50]. NF-κB promotes the expression of pro-inflammatory cytokines [51]. The TNF signaling pathway is primarily involved in biological effects such as cell growth and differentiation, as well as immune regulation. TNF-α is an indispensable immune regulatory factor and a key downstream component of the NF-κB pathway, it

promotes the phosphorylation of AMP-activated protein kinase (AMPK), thereby reducing its inhibitory effect on Myosin Light Chain Kinase (MLCK) and influencing smooth muscle cell contraction and gastrointestinal motility [52]. The HIF-1 signaling pathway is crucial in the body's response to hypoxia or hypoxia stress. HIF-1 α , a key component of this pathway, inhibits the expression of the TLR4/NF-κB pathway and suppresses the release of inflammatory cytokines such as IL-6, IL-1 β , and TNF- α [53]. Relevant studies have confirmed that the PI3K-Akt signaling pathway is a critical node in regulating the intestinal barrier. Phosphorylation of Akt directly inhibits the expression of Occludin, a transcription factor of Zonula Occludens-1 (ZO-1), thereby disrupting the integrity of intercellular junctions in intestinal cells [54]. Inhibiting the PI3K-Akt signaling pathway can achieve protective effects on the intestinal mucosa and alleviate intestinal inflammation [55], thereby exerting therapeutic effects on diarrhea.

This study employed network pharmacology and molecular docking techniques to systematically predict the bioactive components, targets, and signaling pathways of the antidiarrheal effects in alpine bistort rhizome. The results demonstrated that the primary bioactive components of Polygonum cuspidatum are sterol compounds and polyphenols, which exert antidiarrheal functions through multiple target sites and signaling pathways. Molecular docking technology provided preliminary validation, indicating favorable binding effects between the compounds and their targets. However, it should be noted that since these techniques are based on computational simulations, the results require experimental verification. Therefore, future studies should conduct cellular or animal experiments to validate these predictions and further investigate the underlying mechanisms.

5 Conclusion

This study employs multiple methods to analyze 9 categories of components in alpine bistort rhizome. A total of 126 chemical compositions are identified, specifically including 4 polysaccharides, 6 monosaccharides that compose polysaccharides, 3 free sugars, 17 amino acids, 3 nucleosides, 2 sterols, 14 organic acids, 21 flavonoids, 2 glycosides, 1 sugar-conjugated polymer, 34 volatile components, and 19 elements. Among them, the molecular weight of the polysaccharides from alpine bistort rhizome is reported for the first time. Furthermore, 48 compounds are newly discovered in the rhizomes, including 1 sterol, 3 organic acids, 9 flavonoids, 1 glycoside, 1 sugar-conjugated polymer, and 33 volatile components. Meanwhile, based on the chemical composition research results, the potential mechanism of alpine bistort rhizome in treating diarrhea is investigated using network pharmacology and molecular docking methods. The results showed that 50 active components in alpine bistort rhizome could regulate the TNF signaling pathway, lipid and atherosclerosis, PI3K-Akt signaling pathway and HIF-1 signaling pathway by acting on 227 target points, thus exerting the anti-diarrhea effect. The molecular docking results demonstrate that 5 core targets (STAT3, EGFR, TNF, HSP90AA1, and CASP3) exhibit good binding ability with the active compounds. The results unveil that the anti-diarrheal effect of alpine bistort rhizome involves multiple components, targets, and signaling pathways. Future research should further explore its mechanism and validate key targets and signaling pathways, providing a reference for further development and application of alpine bistort rhizome.

Acknowledgements

Not applicable.

Conflicts of Interest

The author of this article, Zhengming Qian, is a member of the editorial office of this journal. All procedures during the editorial review process were

conducted strictly in accordance with the journal's policies, and the author was not involved in handling any part of the process.

Author Contributions

C.Z. and M.W.: Writing-review & editing, Investigation, Data curation, Validation, Supervision, Methodology. Q.H. and Z.H.: Writing-review & editing, Validation, Methodology. J.X.: Writing-review & editing, Validation. W.Y.: Writing-review & editing, Formal analysis. J.F.: Writing-review & editing, Resources. X.S.: Writing-review & editing, Supervision. Z.Q.: Writing-review & editing, Supervision, Resources, Project administration, Funding acquisition. Final approval of the version to be published: All authors. Agreement to be accountable for all aspects of the work in ensuring that questions related to the accuracy or integrity of the work are appropriately investigated and resolved: All authors.

Ethics Approval and Consent to Participate

No ethical approval was required for this article.

Funding

This work was supported by Hubei Provincial Technology Innovation Plan Project (Key R&D Special Project, Grant No. 2025BBB045).

Availability of Data and Materials

The data presented in this study are available on request from the corresponding author.

Supplementary

Not applicable.

References

[1] Mühlmann O, Bacher M, Peintner, U. *Polygonum viviparum* mycobionts on an alpine primary successional glacier forefront. *Mycorrhiza* 2018; 18: 87–95.

[2] He H, Tang C, Cao Z, et al. Revealing Medicinal Constituents of *Bistorta vivipara* Based on Non-Targeted Metabolomics and 16S rDNA Gene Sequencing Technology. *Molecules* 2024; 29(4): 860.

[3] Fan DM, Yang YP. Altitudinal variations in flower and bulbil production of an alpine perennial, *Polygonum viviparum* L. (Polygonaceae). *Plant Biology* 2009; 11(3): 493–497.

[4] Liu GQ, Cao L, Han RC. Plant quercetin degradation by gut bacterium *Raoultella terrigena* of ghost moth *Thitarodes xiaojinensis*. *Frontiers In Microbiology* 2022; 13: 1079550.

[5] Zhou XW, Li LJ, Tian EW. Advances in research of the artificial cultivation of *Ophiocordyceps sinensis* in China. *Critical Reviews in Biotechnology* 2014; 34: 233–243.

[6] Qian ZM, Yang WQ, Chen BY, et al. Comprehensive comparative evaluation of bioactive compound and antioxidant capacity in different parts of *alpine bistort*. *Food Chemistry* 2026; 499: 147288.

[7] Zhang CX, Li YL, Hu FZ. Studies on the chemical constituents from herba *Polygonum viviparum* L. *Natural Product Research and Development* 2005; 17: 177-178.

[8] Vysochina GI, Voronkova MS. Flavonoids of *Bistorta vivipara* (L.) delarbre in relation to their ecological role. *Contemporary Problems of Ecology* 2013; 6(4): 426–433 .

[9] Cheng HW, Lee KC, Cheah KP, et al. *Polygonum viviparum* L. inhibits the lipopolysaccharide-induced inflammatory response in RAW264.7 macrophages through haem oxygenase-1 induction and activation of the Nrf2 pathway. *Journal of The Science of Food And Agriculture* 2013; 93(3): 491-497.

[10] Chang ML, Chang JS, Yu WY, et al. *Polygonum viviparum* L. induces vasorelaxation in the rat thoracic aorta via activation of nitric oxide synthase in endothelial cells. *BMC Complementary and Alternative Medicine* 2014; 14: 150–158.

[11] Qian ZM, Cheng XJ, Wang Q, et al. On-line pre-column FRAP-based antioxidant reaction coupled with HPLC-DAD-TOF/MS for rapid screening of natural antioxidants from different parts of *Polygonum viviparum*. *RSC Advances* 2023; 13(14): 9585-9594.

[12] Bhattacharjee S, Siyad I, Maramattom BV. Chronic diarrhea-the poetic masquerade. *Journal of Postgrad Medicine* 2022; 68(4): 239-242.

[13] Han XY, Liu DF, Guo WS, et al. Clinical study on Zhuyaliao Zhixie Granules combined with Saccharomyces boulardii Sachets in treatment of children with functional diarrhea. *Drugs & Clinic* 2020; 35(9): 1826-1830.

[14] Yu GS, Li CG, Lao HM, et al. Qingchang Zhixie San Application on the Umbilicus Combined with Oral Administration of Zhuyaliao Zhixie Keli for Treating Children's Rotaviral Enteronitis. *Chinese Journal of Coloproctology* 2016; 36(5): 40-42.

[15] Kuang P. Clinical Study on the Treatment of Infantile Diarrhea with Zhuyaliao Zhixie Granules. *Journal of Li-shizhen Traditional Chinese Medicine* 2015; 26(4): 925.

[16] Hu LP, He ZB, Chen BY, et al. A simple, rapid, and green method for determination of three flavonoids in *alpine bistort* rhizome and Zhuyaliao Zhixie Granules by LC-MS/MS. *Journal of Liquid Chromatography & Related Technologies* 2025; online, 1–11.

[17] Li S, Zhang B. Traditional Chinese medicine network pharmacology: Theory, methodology and application. *Chinese Journal of Natural Medicines* 2013; 11: 110–120.

[18] Wang X, Wang ZY, Zheng JH, et al. TCM network pharmacology: a new trend towards combining computational, experimental and clinical approaches. *Chinese Journal of Natural Medicines* 2021; 19 (1): 1–11.

[19] Jiao X, Jin X, Ma Y, et al. A comprehensive application: molecular docking and network pharmacology for the prediction of bioactive constituents and elucidation of mechanisms of action in component-based Chinese medicine. *Computational Biology and Chemistry* 2021; 90: 107402.

[20] Hong M, Li S, Tan HY. et al. A network-based pharmacology study of the herb-induced liver injury potential of traditional hepatoprotective chinese herbal medicines. *Molecules* 2017; 22(4): 632.

[21] Zhang JY, Chen YR,Tang YC. et al. Quality differentiation of Epimedium from different harvesting periods based on LC-MS and network pharmacology. *New Journal of Chemistry* 2024; 48: 9020-9029.

[22] Xiang LI, Liu ZQ, Liao J, et al. Network pharmacology approaches for research of traditional chinese medicines. *Chinese Journal of Natural Medicines* 2023; 21(5): 323-332.

[23] Daina A, Michielin O, Zoete V. SwissADME: a free web tool to evaluate pharmacokinetics, drug-likeness and medicinal chemistry friendliness of small molecules. *Scientific Report* 2017; 7: 42717.

[24] Xing N, Qin J, Ren DS, et al. Integrating UPLC-Q-Exactive Orbitrap/MS, network pharmacology and experimental validation to reveal the potential mechanism of Tibetan medicine Rhodiola granules in improving myocardial ischemia-reperfusion injury. *Journal of Ethnopharmacology* 2023; 314: 116572.

[25] Zhang LX, Dong J, Wei H, et al. TCMSID: a simplified integrated database for drug discovery from traditional Chinese medicine. *Journal of Cheminformatics* 2022; 14(1): 89.

[26] BI XY, Wang YY, Wang JH, et al. Machine learning for multi-Target drug discovery: challenges and opportunities in systems pharmacology. *Pharmaceutics* 2025; 17(9): 1186.

[27] DAINA A, MICHIELIN O, ZOETE V. SwissTargetPrediction: updated data and new features for efficient prediction of protein targets of small molecules. *Nucleic Acids Research* 2019; 47(1): 357-364.

[28] Liu ZY, Huang HL, Yu Y, et al. Exploring the potential molecular mechanism of the Shugan Jieyu Capsule in the treatment of depression through network pharmacology, molecular docking, and molecular dynamics simulation. *Current Computer-Aided Drug Design* 2024; 20(5): 501-517.

[29] Huang Q, Yang WQ, Li XF, et al. Screening of α -Glucosidase Inhibitors in Extracts of Polygonum bistorta Based on Spectrum-Effect Relationship. *Journal of Experimental and Clinical Application of Chinese Medicine* 2024; 5(4): 69-81.

[30] Man JY, Liu Y, Xing XY, et al. Optimization of Extraction Process of Polysaccharides from *Polygonum viviparum* L. by Response Surface Methodology. *China Animal Husbandry & Veterinary Medicine* 2025; 52(3): 1416-1427.

[31] Lu ZH, Wu XL, Liu F. Comparative Analysis of Nutritional Components in Forage of Host Hepialus Larvae of Cordyceps sinensis. *Southwest China Journal of Agricultural Sciences* 2013; 26(5): 2048-2051

[32] Chen SJ, Zeng W, Yin DH. Analysis of Trace Elements in the Rhizome of *Polygonum viviparum* . *Special Wild Economic Animal and Plant Research* 1994; 3: 61-62.

[33] He H, Tang C, Cao Z, et al. Revealing Medicinal Constituents of Bistorta vivipara Based on Non-Targeted Metabolomics and 16S rDNA Gene Sequencing Technology. *Molecules* 2024; 29(4): 860.

[34] Isken O, Langerwisch U, Schönherr R, et al. Functional characterization of bovine viral diarrhea virus nonstructural protein 5A by reverse genetic analysis and live cell imaging. *Journal Of Virology* 2014; 88(1): 82-98.

[35] Lee KN, Lee OY. Intestinal microbiota in pathophysiology and management of irritable bowel syndrome. *World Journal of Gastroenterology* 2014;20(27): 8886-8897.

[36] Sui XN, Han XB, Wang XB, et al. 2-Nonanol produced by Bacillus velezensis EM-1: a new biocontrol agent against tobacco brown spot. *Frontiers in Microbiology* 2025; 16: 1582372.

[37] Faubel N, Makran M, Barberá R, et al. Anti-inflammatory activity of plant sterols in a co-culture model of intestinal inflammation: focus on food-matrix effect. *Food & Function* 2024; 17;15(12): 6502-6511.

[38] Choi JN, Choi YH, Lee JM, et al . Anti-inflammatory effects of beta-sitosterol-beta-D-glucoside from Trachelospermum jasminoides(Apocynaceae) in lipopolysaccharide-stimulated R AW 264. 7 murine macrophages . *Natural Product Research* 2012; 26(24) : 2340-2343.

[39] Zhu XY, Qiao TL, Huang ZQ, et al. Caffeic acid improves intestinal barrier function integrity through activation of Nrf2 signaling pathway in weaned piglets and H2O2 induced IPEC-J2 cells. *Journal of Nutritional Biochemistry* 2025; 143:109952.

[40] Su XR, Zhu ZH, Zhang L, et al. Anti-inflammatory property and functional substances of Lonicerae Japonicae Caulis. *Journal of Ethnopharmacology* 2021; 267: 113502.

[41] Jie H, Arianne L. T, Stat3: Friend or Foe in Colitis and Colitis-associated Cancer?. *Inflammatory Bowel Diseases* 2014; 20(12): 2405-2411.

[42] Ho J, Moyes D L, Tavassoli M, et al. The role of ErbB receptors in infection. *Trends Microbiol* 2017; 25(11): 942-952.

[43] Bowen J M, Mayo B J, Plews E, et al. Determining themechanisms of lapatinib-induced diarrhoea using a rat model. *Cancer Chemother Pharmacol* 2014; 74(3): 617-627.

[44] Darkoh C, Comer L, Zewdie G, et al . Chemotactic chemokines are important in the pathogenesis of irritable bowel syndrome. *PLoS One* 2014; 9(3): e93144.

[45] Yan S., Li Y. Z., Zhu X. et al. HuGE systematic reviewand meta-analysis demonstrate association of CASP-3 and CASP-7 genetic polymorphisms with cancer risk. *Genetics and Molecular Research* 2013; 12(2): 1561-1573.

[46] Zheng M, Jia Z, Wang P, et al . Bioinformatics analysis and experimental validation reveal that heat HSP90AA1 enhances intestinal ischemia reperfusion induced necroptosis by inducing phosphorylated MLKL. S*cientific Reports* 2025; 15(1): 38698.

[47] Liu C, Liu Y, Liang L, et al. RNA-Seq based transcriptome analysis during bovine viral diarrhoea virus (BVDV) infection. *BMC Genomics* 2019; 20(1): 774.

[48] Yu T, Wu L, Zhang T, et al. Insights into Q-markers and molecular mechanism of Sanguisorba saponins in treating ulcerative colitis based on lipid metabolism regulation. *Phytomedicine* 2023; 116: 154870.

[49] Suo XY, Fan GQ, Li B, et al. PEDV infection alters host lipid metabolism. *Chinese Journal of Veterinary Science* 2024; 44(06): 1107-1112.

[50] Yin HH, Liu W, Ji XY, et al. Study on the mechanism of Wumei San in treating piglet diarrhea using network pharmacology and molecular docking. *Frontiers in Veterinary Science* 2023; 10: 1138684

[51] Chen MY, Meng XF, Han YP, et al. Profile of crosstalk between glucose and lipid metabolic disturbance and diabetic cardiomyopathy:Inflammation and oxidative stress. *Frontiers in Endocrinology* 2022; 13: 983713.

[52] NALLI A D, KUMA R D P, MAHAVADI S, et al . Hypercontractility of intestinal longitudinal smooth muscle induced by cytokines is mediated by the nuclear factor- κ B/AMPactivated kinase /myosin light chain kinase pathway . *Journal of Pharmacology and Experimental Therapeutics* 2014; 350(1) : 89-98.

[53] Wei H, Xu YX, Qin l, et al. Protective mechanism of HIF-1 α on myocardial injury in rats with myocardial ischemia-reperfusion by TLR4/NF- κ B signaling pathway. *Journal of Clinical and Experimental Medicine* 2019; 18(10): 1017-1020.

[54] Wang HO, Huang WK, Pan XY, et al. Quzhou Aurantii Fructus Flavonoids Ameliorate Inflammatory Responses, Intestinal Barrier Dysfunction in DSS-Induced Colitis by Modulating PI3K/AKT Signaling Pathway and Gut Microbiome. *Journal of Inflammation Research* 2025; 18: 1855-1874.

[55] Zhan JY, Yuan XX, Wang BY, et al. Effects of Liancao-Xieli capsule on intestinal mucosal inflammatory factors and TLR4/PI3K/Akt/ mTOR signaling pathway in mice with ulcerative colitis. *Journal of Hainan Medical University* 2021; 27: 1872–1877.